Chapter 6

Emerging Superconductivity and Topological States in Bismuth Chalcogenides

Jifeng Shao and Wenka Zhu

Additional information is available at the end of the chapter

http://dx.doi.org/10.5772/intechopen.73057

Abstract

In this chapter, we review the recent experimental work in emerging superconductors, i.e., bismuth chalcogenides, including the newly discovered $BiS(e)_2$-based layered superconductors and some topological superconductor candidates. Their crystal structure and various physical properties are reviewed in detail, with the correlation between structure and superconductivity as the main clue throughout this chapter. Bi_2OS_2 is the simplest structure in Bi—O—S compounds and probably the parent compound of this series. Superconductivity emerges when carriers are introduced by intercalation or chemical substitution. The superconducting layer is extended to $BiSe_2$ layer in $LaO_{1-x}F_xBiSe_2$, which has an improved superconductivity. Moreover, the topological insulator Bi_2Se_3 can be turned into superconductors by intercalating metal atoms into van der Waals space, e.g., $Sr_xBi_2Se_3$, a potential topological superconductor, whose quantum oscillations reveal a possible topological surface state. The intermediate external pressure can efficiently suppress superconductivity, which reemerges when pressure is further increased, while T_c is nearly invariant in high-pressure region, indicating an unconventional pairing state.

Keywords: bismuth chalcogenides, $BiS(e)_2$-based superconductors, crystal structure, intercalation, topological superconductors, high pressure

1. Introduction

Superconductivity was first discovered in the resistivity measurement of mercury by Kamerlingh Onnes in 1911. Its resistance abruptly vanishes at 4.1 K. Zero resistance means no energy loss in electric transport, which could greatly solve the energy crisis in the future. Since then, superconductivity has been a long-lasting hot topic in condensed matter physics. Exploring room temperature superconductors is one of the ultimate dreams.

However, so far, only two kinds of unconventional superconducting systems have exceeded the Macmillan limit at ambient pressure, i.e., the cuprate and iron-based superconductors. In general, the correlation of structure and typical properties is always a useful guideline for effectively searching for special functional materials. In fact, the structure of both cuprate and iron-based superconductors can be characterized as a sandwiched "hamburger" model. It consists of superconducting layers (CuO_2 plane, Fe_2M_2 (M = As, P, S, Se, and Te) layer) and spacer layers, which stack alternatively along the c-axis [1, 2]. Superconductivity occurs when the charged carriers are generated by the defects or substitution in superconducting layers or more commonly provided by the space layers; namely, a new superconducting layer probably means a new superconducting system. The spacer layer can be easily tuned by doping, substitution, intercalation, and pressure, which could affect superconductivity [3]. Therefore, materials with layered structure have been regarded as the most promising playground for exploring new high-T_c superconductors.

In 2010, superconductivity arising from the topological insulator Bi_2Se_3 by Cu intercalation was first reported [4]. It has drawn much attention since $Cu_xBi_2Se_3$ is proposed as a topological superconductor candidate, as evidenced by the zero-bias conductance peak and quantum oscillation experiment [5, 6]. Very recently, superconductivity with topological states was also reported in its isostructural compounds, $Sr_xBi_2Se_3$ and $Nb_xBi_2Se_3$ [7, 8]. In 2012, an exotic superconductivity was discovered in a new layered structure $Bi_4O_4S_3$ with zero-resistance superconducting temperature at about 4.5 K [9]. Soon, another new BiS_2-based superconductor $LaO_{0.5}F_{0.5}BiS_2$ was reported, whose structure is more definite and the zero-resistance superconducting temperature is about 8 K for the samples annealed under high pressure [10]. As its structure is very similar to the iron-based superconductor LaOFeAs, this system has been intensively researched, and lots of isostructural superconductors have been synthesized, including $ReO_{1-x}F_xBiS_2$ (Re: Ce, Pr, Nd, Yb), $Sr_{1-x}Re_xFBiS_2$ (Re: La, Ce), $EuBiS_2F$, and $Eu_3Bi_3S_4F_4$ [11–15]. These researches are focused on tuning the spacer layers. The attempts to explore new superconducting layers only succeed in $LaO_xF_xBiSe_2$ and $Sr_{0.5}La_{0.5}FBiSe_2$ [16–18]. So far, the superconducting layer of this system has been extended to $BiCh_2$ (Ch: S, Se). In this chapter, the crystal structure and superconducting properties of Bi—O—S superconductors, $LaO_{1-x}F_xBiSe_2$ single crystals, and $Sr_xBi_2Se_3$ single crystals are briefly reviewed.

2. Crystal structure and superconducting properties

2.1. Bi—O—S superconductors

The element composition of $Bi_4O_4S_3$ is the same as $Bi_4O_4(SO_4)_xBi_2S_4$ (x = 0.5), and its parent $Bi_6O_8S_5$ is an oxide insulator composed of alternatively stacked BiS_2 and $Bi_2O_2 + SO_4 + Bi_2O_2$ layers along the c-axis. It has a tetragonal structure with I4/mmm space group and its schematic crystal structure is shown in **Figure 1(c)**. Band calculations demonstrate that the half vacancy of SO_4 layer generates electron carriers into BiS_2 layer. The normal state of $Bi_4O_4S_3$ is metallic and the superconductivity mainly originates from the Bi $6p_x$ and $6p_y$ orbitals in BiS_2 layers. Therefore, the BiS_2 layer is called the superconducting layer in this family.

http://dx.doi.org/10.5772/intechopen.73057

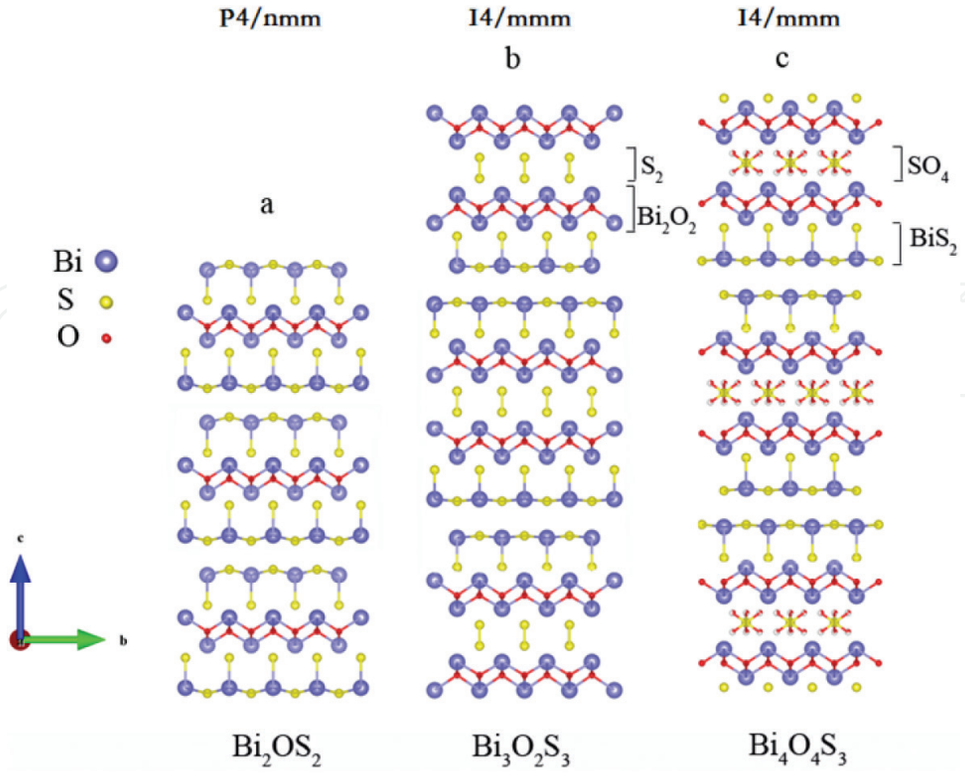

Figure 1. Crystal structures of (a) Bi_2OS_2, (b) $Bi_3O_2S_3$, and (c) $Bi_4O_4S_3$ [21].

However, the chemical composition studies show that it probably contains two new Bi—O—S phases, i.e., Bi_2OS_2 and $Bi_3O_2S_3$. Their schematic structures can be seen in **Figure 1(a)** and **(b)**. Bi_2OS_2 is an insulating phase and its content is less than 10%. $Bi_3O_2S_3$ is the main phase and likely accounts for the 4.5 K superconductivity in $Bi_4O_4S_3$. And the superconductivity can be suppressed by the amount of Bi_2OS_2-like stacking faults [19]. Once the quality of $Bi_3O_2S_3$ sample is improved, the superconducting volume fraction will be enhanced with its zero-resistance superconducting temperature increased up to 4.9 K [20].

The crystal structure of $Bi_3O_2S_3$ is similar to $Bi_4O_4S_3$ with the same I4/mmm space group, a = 3.9674 Å and b = 41.2825 Å. The electron carriers are believed to be generated from S_2^{2-} layers replacing the vacancy of SO_4^{2-} layers in $Bi_4O_4S_3$. The chemical composition of Bi_2OS_2 can also be expressed as $BiOBiS_2$. Then we can see it is isostructural with $LaOBiS_2$ with P4/nmm space group, a = b = 3.9744 Å and c = 13.7497 Å. $BiOBiS_2$ has the simplest structure and composition, then it is probably the parent compound of this BiS_2-based family. Besides, superconductivity is likely to be induced by introducing carriers into spacer layer. In fact, F-doped Bi_2OS_2 has been reported to exhibit bulk superconductivity below 5 K [21, 22].

Figure 2 shows the powder XRD patterns of $Bi_3O_2S_3$, $BiO_{1-x}F_xBiS_2$, and Bi_2OS_2 samples. We can see that samples of Bi—O—S compounds tend to contain impurities such as Bi_2O_3, Bi, and Bi_2S_3, because their synthesis temperature is relatively low (520°C for $Bi_4O_4S_3$ and $Bi_3O_2S_3$, and 400°C for $Bi_2(O,F)S_2$) [9, 19–21]. Besides, these samples can only be synthesized in a narrow temperature region. Another difficulty in detecting their actual composition and structure is that several strong diffraction peaks in the powder XRD patterns are very close to each other.

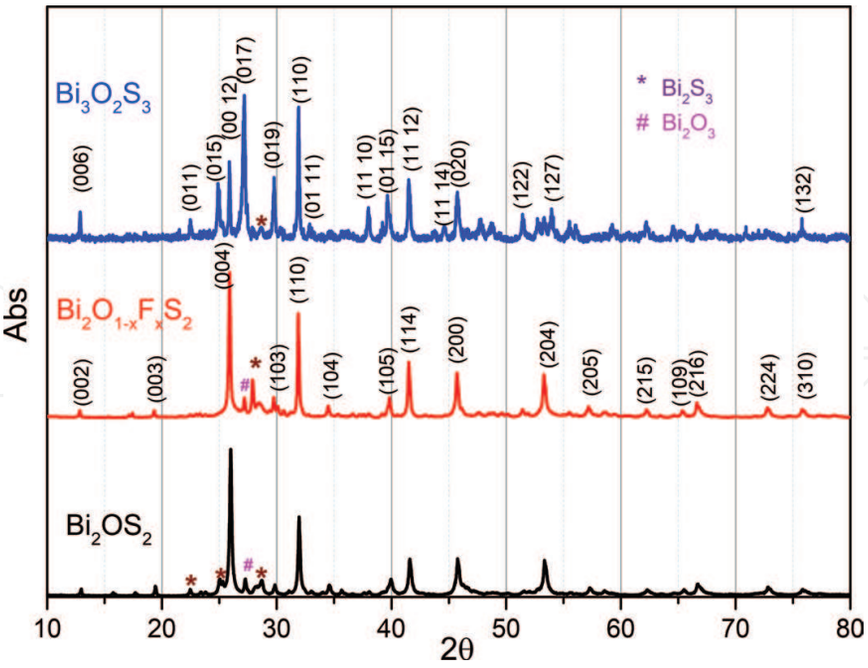

Figure 2. Powder XRD patterns of $Bi_3O_2S_3$, Bi_2OS_2, and $Bi_2O_{1-x}F_xS_2$ polycrystalline samples. The special characters (*, #) represent the impurity phases.

Hence, bulk superconductivity is very important in this system. Up to now, high-quality samples, especially single crystals, are still needed to investigate the relationship of structure and properties, in view of the multiple competing low-energy crystal structures in this system.

The physical properties of Bi—O—S superconductors are introduced, taking $Bi_3O_2S_3$ and F-doped Bi_2OS_2 for instance [20, 21]. **Figure 3(a)** shows the temperature dependence of resistivity and magnetoresistivity under different applied magnetic fields for $Bi_3O_2S_3$. Its normal state is metallic-like and a sharp drop in resistivity appears at 5.8 K and quickly down to zero at 4.9 K. The upper critical field is estimated from resistivity versus temperature curves under different applied magnetic fields perpendicular to the sample surface, as seen in the insets of **Figure 3(a)**. According to the Werthamer-Helfand-Hohenberg (WHH) formula, the upper critical field $\mu_0 H_{c2}(0)$ is evaluated to be about 4.84 T.

The shielding volume fraction is about 100%, revealing bulk superconductivity, as seen in **Figure 3(b)**. The divergence in temperature dependence of magnetic susceptibility and the M-H curves characterize $Bi_3O_2S_3$ as a type-II superconductor. The Hall effect shows a remarkable nonlinear magnetic field dependence of transverse resistivity, which means it is likely a multiband superconductor [23]. However, the Hall resistivity at different temperatures is all negative, indicating that the dominant charge carriers are electron-type. The evaluated charge carrier density is about 1.5×10^{19} cm^{-3}. It is much lower than those of cuprate and iron-based superconductors, implying a low superfluid density. Chemical substitution effects seem to increase the charge carrier density, but ultimately inhibit the superconductivity [24–26].

A clear specific heat anomaly appears around the superconducting transition temperature, as seen in **Figure 3(d)**, confirming the bulk superconductivity in $Bi_3O_2S_3$. The electronic specific

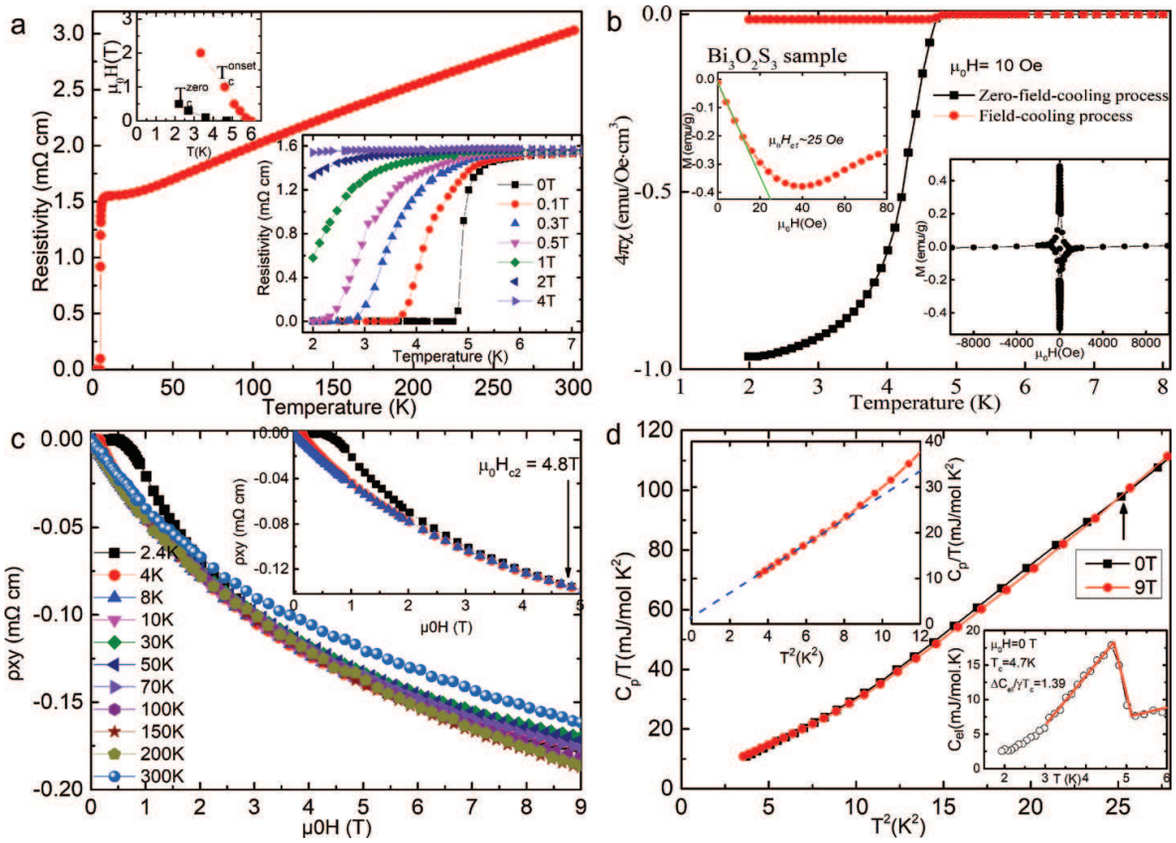

Figure 3. (a) Temperature dependence of resistivity for $Bi_3O_2S_3$. The lower inset shows the curves of resistivity versus temperature under different applied magnetic fields and the upper inset shows the field dependence of T_c^{onset} and T_c^{zero}. (b) Temperature dependence of magnetic susceptibility for $Bi_3O_2S_3$ and the insets show the magnetic field dependence of magnetic susceptibility at 2 K. (c) Hall resistivity versus magnetic field at different temperatures. (d) Curves of C/T versus T^2 in superconducting state (0 T) and normal state (9 T). The upper inset shows the data of normal state at low temperature region. The lower inset shows the temperature dependence of calculated electron specific heat in superconducting state [20].

heat coefficient γ and phonon specific heat coefficient β for the normal state under 9 T are obtained as 1.65 mJ/(mol K^2) and 2.6 mJ/(mol K^4), respectively, using linear fitting of C/T versus T^2. As the phononic contribution to the heat capacity is generally independent of the external magnetic field, the electronic specific heat of superconducting state can be expressed by the equation

$$C_e(T) = C(T, H = 0) - C(T, H = 9T) + \gamma T. \quad (1)$$

The estimated value of $\Delta C_e/\gamma T_c$ is comparable to the BCS weak-coupling limit 1.43.

Undoped Bi_2OS_2 was predicted to be an insulating oxide by the band structure calculations. However, we can see it is almost metallic from 300 K to 30 K, and a weak semiconductor behavior emerges below 30 K, which may be originating from the impurities. The F-doping can significantly decrease the normal state resistivity and increase the shielding volume fraction, as shown in **Figure 4**. The best doping ratio is about 0.24. From the temperature dependence of magnetic susceptibility, the best doped sample has a bulk type-II-like

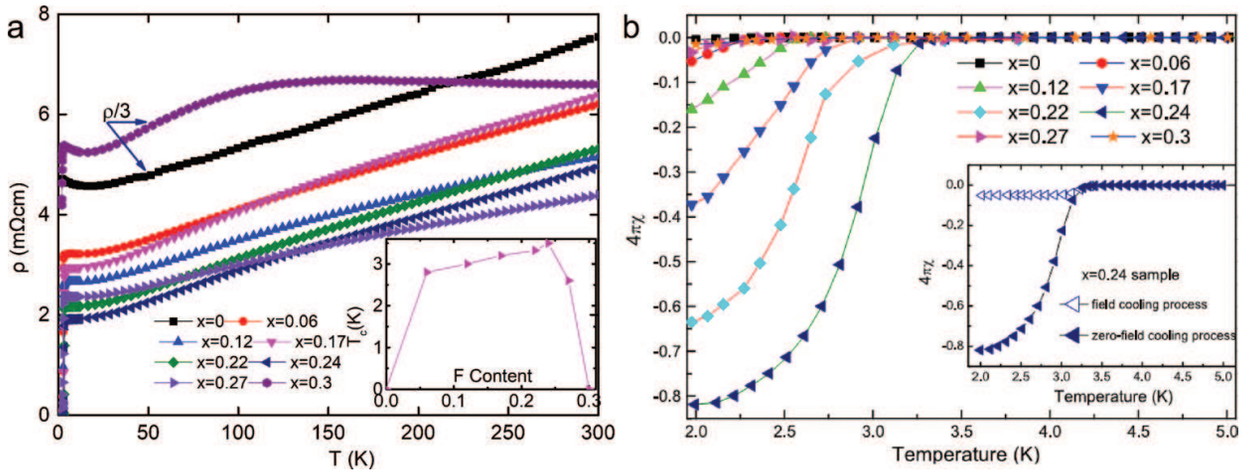

Figure 4. (a) Temperature dependence of resistivity for $BiO_{1-x}F_xBiS_2$. The inset shows the variation of T_c with different F-doping content. (b) Temperature dependence of magnetic susceptibility for $BiO_{1-x}F_xBiS_2$ under ZFC process. The inset presents the FC and ZFC data for x = 0.24 sample [21].

superconductivity. When doping content exceeds 0.27, superconductivity disappears and the resistivity increases quickly. Besides, the quality of samples (x > 0.27) synthesized by conventional solid state reaction method begins to deteriorate with increasing doping content [21]. In fact, the $Bi_2(O,F)S_2$ samples synthesized by topotactic fluorination using XeF_2 also contain bismuth impurity [22]. It is difficult to get pure samples because the optimal synthesis temperature is only around 400°C.

2.2. Re(O,F)BiCh$_2$ (Ch: S, Se) superconductors

$Re(O,F)BiS_2$ (Re: La, Ce, Pr, Nd, Yb) superconductors have been intensively studied since the report of $LaO_{0.5}F_{0.5}BiS_2$. Their structure is more definite and similar to "1111" phase of iron-based superconductors. Single crystals of this structure have been successfully synthesized [27]. Structure tuning is mainly concentrated on the spacer layers rather than the superconducting layer. And only the electron-doping into the insulating parent can induce superconductivity [28]. Here, we introduce the crystal structure and various physical properties of $LaO_{1-x}F_xBiSe_2$ single crystals, which also firstly extend the superconducting layer to $BiSe_2$ layer.

The powder XRD pattern and crystal structure of $LaO_{0.59}F_{0.41}BiSe_2$ superconducting single crystal are presented in **Figure 5**. No impurity phase is found and each peak is indexed. It has a P4/nmm tetragonal lattice with the refined lattice constants a = b = 4.1377 Å and c = 14.1566 Å, which are larger than those of $LaO_{0.5}F_{0.5}BiS_2$ for the larger ionic radius of Se^{2-}. **Figure 6** shows a comparison of the temperature dependence of resistivity for $La(O,F)BiS_2$ and $La(O,F)BiSe_2$ samples. $LaOBiS_2$ can be described as an insulator while $LaOBiSe_2$ is metallic. For $LaO_{0.5}F_{0.5}BiS_2$, it exhibits a semiconducting behavior before the superconducting transition begins. The transport property of $LaO_{0.5}F_{0.5}BiSe_2$ is similar to $Bi_3O_2S_3$ but with a lower residual resistivity. Other isostructural compounds such as $LaO_{0.5}F_{0.5}BiTe_2$ and $LaO_{0.5}F_{0.5}SbS_2$ are also reported, but no superconductivity can be observed down to 1.7 K [16].

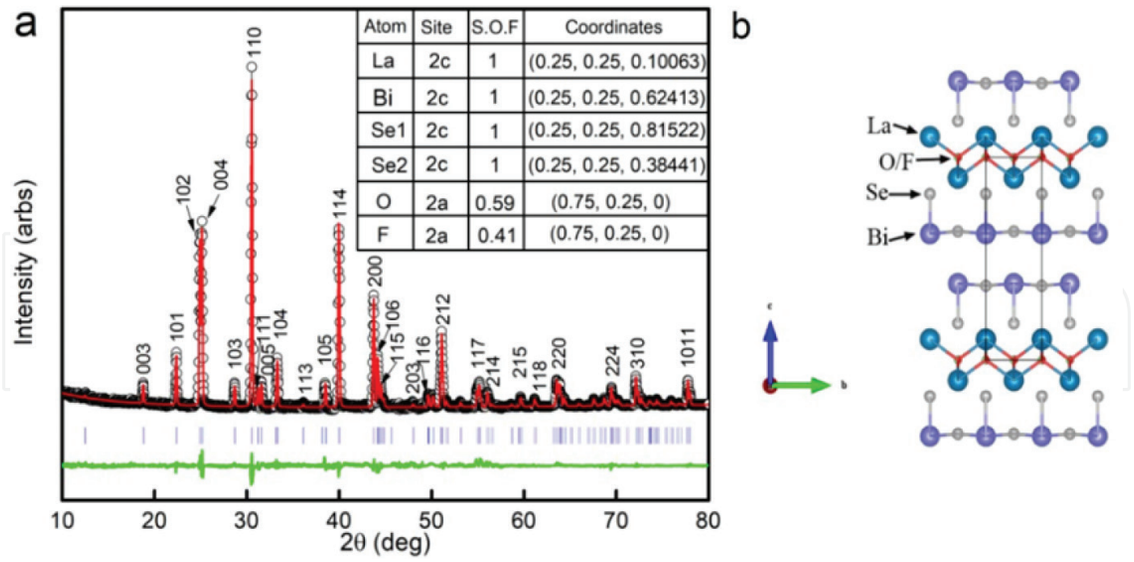

Figure 5. (a) Powder XRD pattern (black circles) with the Rietveld refinement (red curve) and Miller indices for $LaO_{0.59}F_{0.41}BiSe_2$. The inset table summarizes the structural parameters. (b) Crystal structure of $LaO_{0.59}F_{0.41}BiSe_2$. The rectangle indicates the unit cell [17].

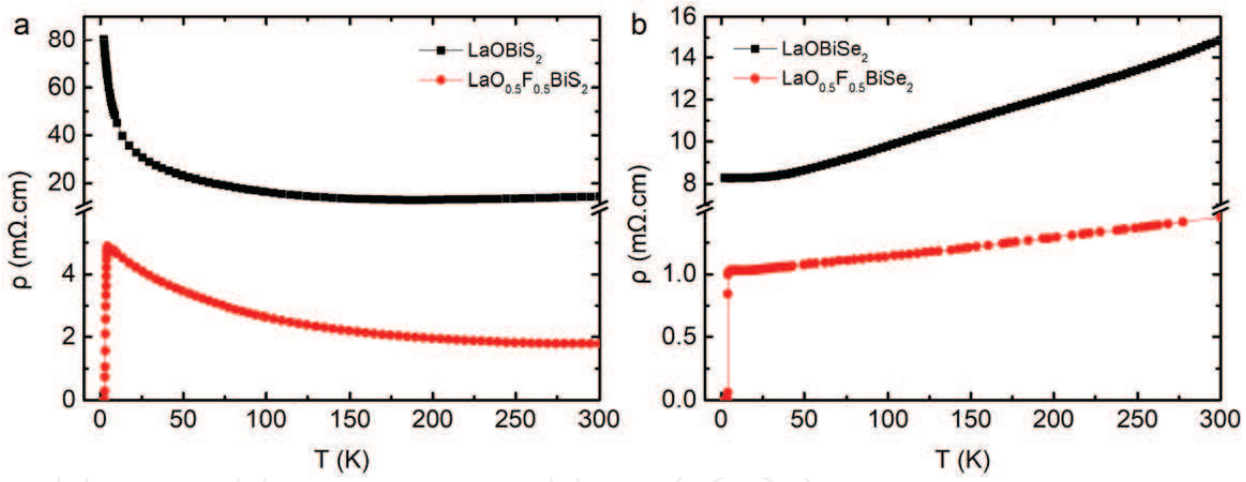

Figure 6. A comparison of the temperature dependence of resistivity between (a) $La(O,F)BiS_2$ and (b) $La(O,F)BiSe_2$.

Fluorine doping effect on the superconductivity of $LaO_{1-x}F_xBiSe_2$ single crystals is shown in **Figure 7(a)** and **(b)**. F-doping can significantly decrease the resistivity of normal state and increase the superconducting transition temperature and shielding volume fraction. Unfortunately, the flux method can only grow single crystals with the largest F content of about 0.5. For example, the sample with F-doping amount of 0.52 was grown by a nominal component of 0.9. The magnetic susceptibility measurement shows $LaO_{1-x}F_xBiSe_2$ has a bulk superconductivity and belongs to the type-II superconductors. Upper critical magnetic field can be evaluated from the resistivity versus temperature under various magnetic fields. As seen in **Figure 7(c)** and **(d)**, the upper critical fields at zero temperature are estimated to be 29 T and 1 T for H||ab and H⊥ab, respectively, which indicate large anisotropy.

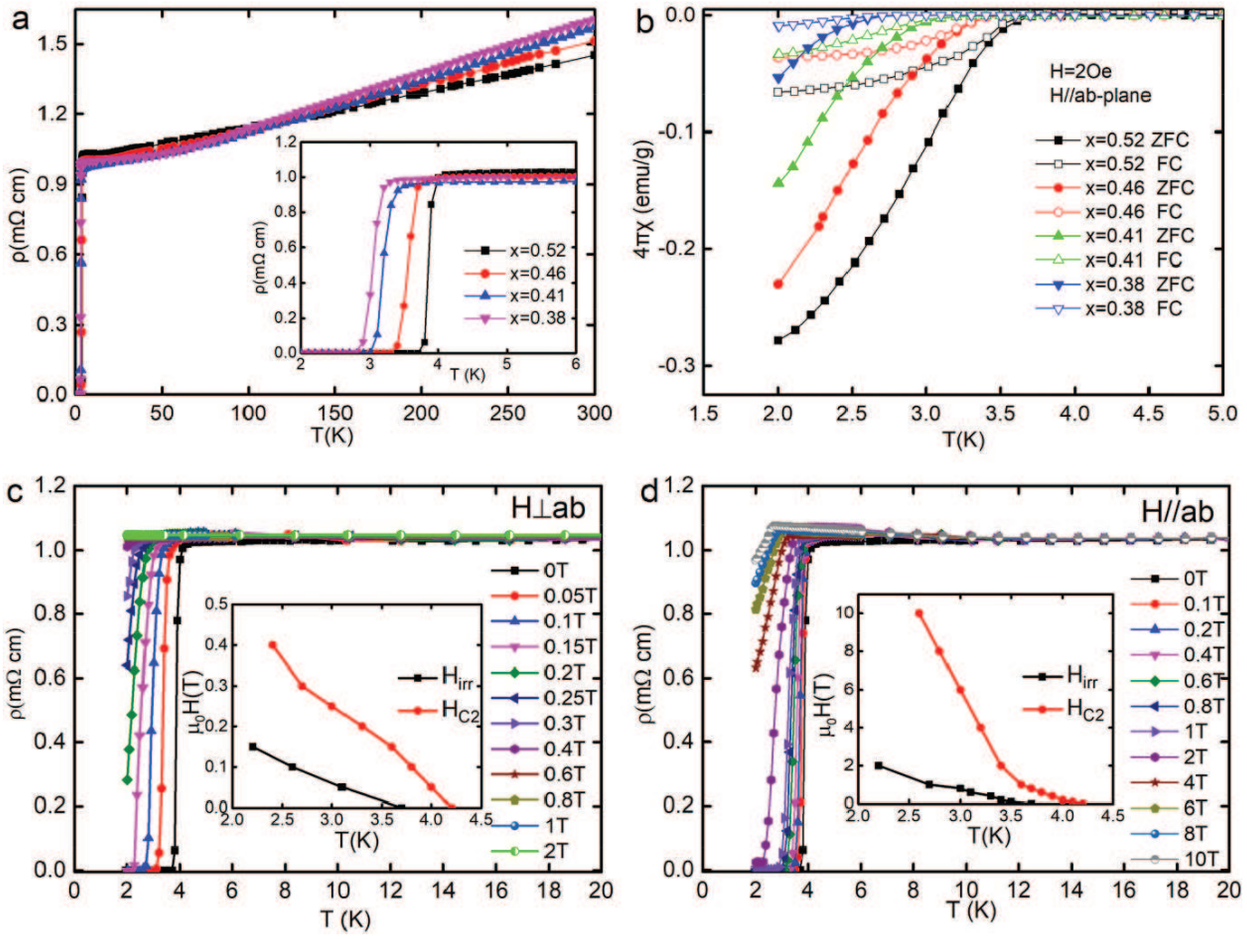

Figure 7. Superconducting properties of $LaO_{1-x}F_xBiSe_2$ single crystals with different F-doping contents. (a) Temperature dependence of resistivity and an enlarged view near the superconducting transition temperature for all samples. (b) ZFC and FC magnetic susceptibility versus temperature with magnetic field applied parallel to ab-plane for all samples. (c) and (d) Resistivity versus temperature with magnetic field applied perpendicular to and parallel to ab-plane, respectively, for the x = 0.52 sample [17].

The anisotropy parameter γ_s of the $LaO_{1-x}F_xBiSe_2$ superconducting single crystal is investigated by measuring the angular dependence of resistivity under various magnetic fields at 3 K (see **Figure 8**). Note that the angle θ describes the deviation of magnetic field with respect to the ab-plane of single crystal. Only the data with magnetic field below 1 T are selected for the reduced magnetic field, because the $H_{C2}(0)$ for H⊥ab is about 1 T. The reduced magnetic field is calculated by the equation

$$H_{red} = H\sqrt{\sin^2\theta + \gamma_s^{-2}\cos^2\theta}. \quad (2)$$

According to the Ginzburg-Landau theory [29], the curves of resistivity versus reduced magnetic field under different magnetic fields should merge into one. The resultant anisotropy parameter at 3 K is about 30 (see **Figure 8(b)**), which is close to the result of upper critical field within the ab-plane.

Considering that the T_c of $LaO_{0.5}F_{0.5}BiS_2$ is increased from 2.7 K to 10.6 K under a hydrostatic pressure of 1.68 GPa [30], the highest T_c among the BiS_2-based superconductors, higher T_c, above 10.6 K

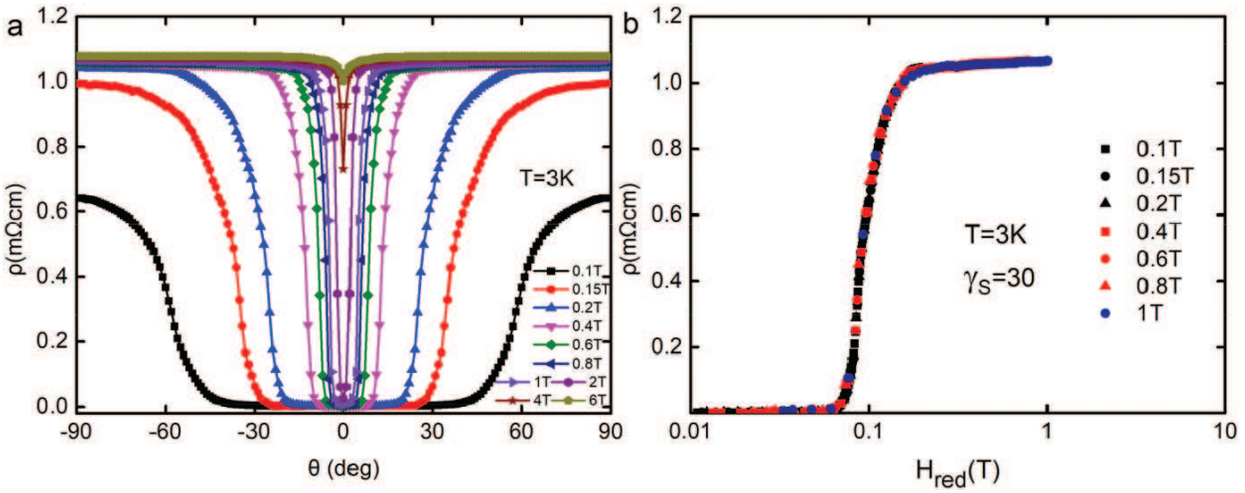

Figure 8. Anisotropy of $LaO_{1-x}F_xBiSe_2$ superconducting single crystal. (a) Angular dependence of resistivity taken under magnetic fields from 0.1 T to 6 T at 3 K for $LaO_{0.48}F_{0.52}BiSe_{1.93}$ single crystal. (b) Scaling of the resistivity vs. the reduced magnetic field H_{red} [17].

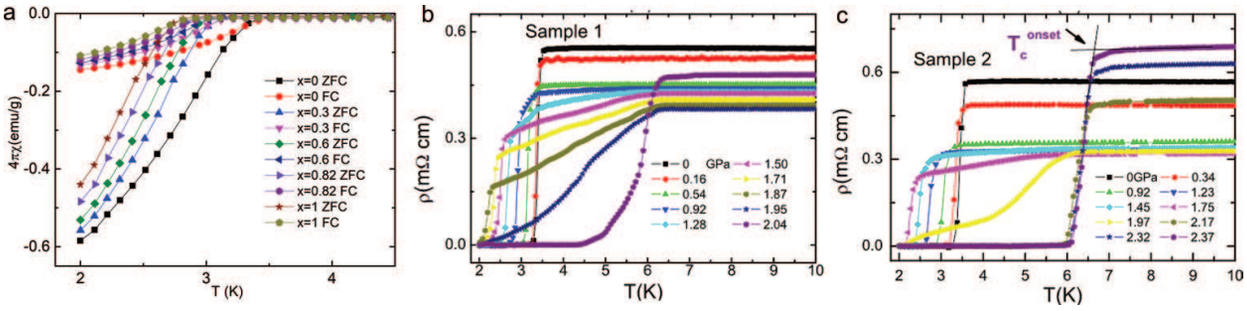

Figure 9. High-pressure effect on the superconductivity of $LaO_{0.5}F_{0.5}BiSe_2$ single crystal. (a) High-pressure effect on the temperature dependence of magnetic susceptibility. (b) and (c) High-pressure effect on the transport properties of two single crystal samples of $LaO_{0.5}F_{0.5}BiSe_2$ [31].

is expected for $LaO_{0.5}F_{0.5}BiSe_2$ under external pressure since its zero-resistance temperature is about 3.5 K. However, we find that its superconductivity and shielding volume fraction decrease unexpectedly with increasing pressure below 1 GPa hydrostatic pressure, as seen in **Figure 9(a)**. Another experiment with higher pressure shows that a new superconducting phase emerges at about 1.2 GPa and T_c reaches about 6.5 K at 2.17 GPa [31]. Accompanied by this crossover, the normal state is switched from that with a low temperature resistivity upturning to a metallic one. Accordingly, the normal state resistivity also shows a nonmonotonic change with the external pressure. These facts suggest that the $BiSe_2$-based system is very different from the BiS_2-based system.

2.3. $M_xBi_2Ch_2$ (Ch: Se, Te) superconductors

Topological insulator has linearly dispersive band structures and its topological surface state exhibits metallic properties while the bulk state is insulating. If its spin-momentum locking effect combines with superconductivity, Majorana fermion may exist, which is useful for quantum computing. At first, the topological superconductors were mostly focused on the proximity-induced

superconductivity. The discovery of $Cu_xBi_2Se_3$ superconductor opens a new gate to topological superconductors, i.e., superconductors induced by doping into topological insulators, which are expected to be the candidate of three-dimensional topological superconductors. Recently, a series of superconductors based on the topological insulators have been reported, such as $Cu_x(PbSe)_5(Bi_2Se_3)_6$ [32], $Sr_xBi_2Se_3$ [7], $Nb_xBi_2Se_3$ [8], and $Tl_xBi_2Te_3$ [33]. Here, we put emphasis on the crystal structure and physical properties of $Sr_xBi_2Se_3$ single crystals.

The structure of $Sr_xBi_2Se_3$ is similar to that of $Cu_xBi_2Se_3$ and isomorphic to the parent Bi_2Se_3. Sr atoms may act as a bipolar dopant that can be embedded in the van der Waals space or randomly substitute for Bi. The actual Sr doping content of $Sr_xBi_2Se_3$ is very little so that it is hard to define its precise position. Nevertheless, the lattice constants of $Sr_xBi_2Se_3$ are a little larger than those of Bi_2Se_3, while the lattice constants of $Bi_{2-x}Sr_xSe_3$ are smaller. The c-axis lattice constant of $Bi_{2-x}Sr_xSe_3$ decreases slightly with increasing doping content (see **Figure 10(b)**). In addition, all samples grown in $Bi_{2-x}Sr_xSe_3$ ratio show no signs of superconductivity at 1.8 K, as seen in **Figure 11(a)**. Therefore, we could use **Figure 10(a)** as the schematic structure diagram.

The linear curves of Hall resistivity versus magnetic field indicate that $Sr_xBi_2Se_3$ has only one electron-like bulk carrier. The carrier density increases slightly with decreasing temperature. Its average is around 2.3×10^{19} cm^{-3}, about 1–2 orders of magnitude lower than $Cu_xBi_2Se_3$. **Figure 11(d)** and **(e)** shows that the T_c of superconducting samples changes little with different Sr contents, but the shielding volume fraction is very different. Only those samples with Sr content above 0.06 have a large shielding volume fraction. Moreover, the superconductivity is very stable in air, as evidenced by the almost unchanged shielding volume fraction for the sample placed in air even for a month. This provides great convenience for experimental research.

The topological surface state of $Sr_xBi_2Se_3$ single crystal has been investigated through Shubnikov-de Haas oscillation measurements. Clear oscillations in resistivity and Hall resistivity can be observed under high magnetic field at different temperatures, as shown in **Figure 12(a)** and **(c)**. The oscillation amplitudes become more pronounced for higher magnetic field and lower temperature. However, the oscillatory periods measured at different temperatures remain constant, so only the data at 0.35 K with the most noticeable oscillations are selected to deduce the Landau level

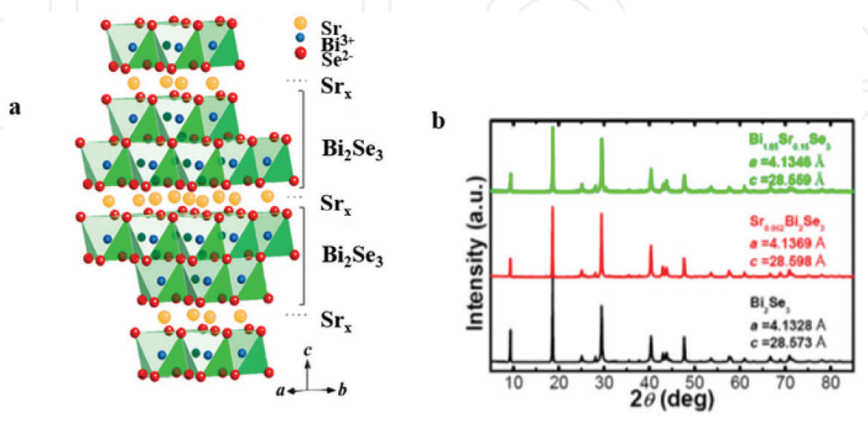

Figure 10. Crystal structure of $Sr_xBi_2Se_3$ superconductors. (a) Schematic diagram of $Sr_xBi_2Se_3$ crystal structure. (b) Powder XRD patterns of $Sr_xBi_2Se_3$, Bi_2Se_3, and $Bi_{2-x}Sr_xSe_3$ [7].

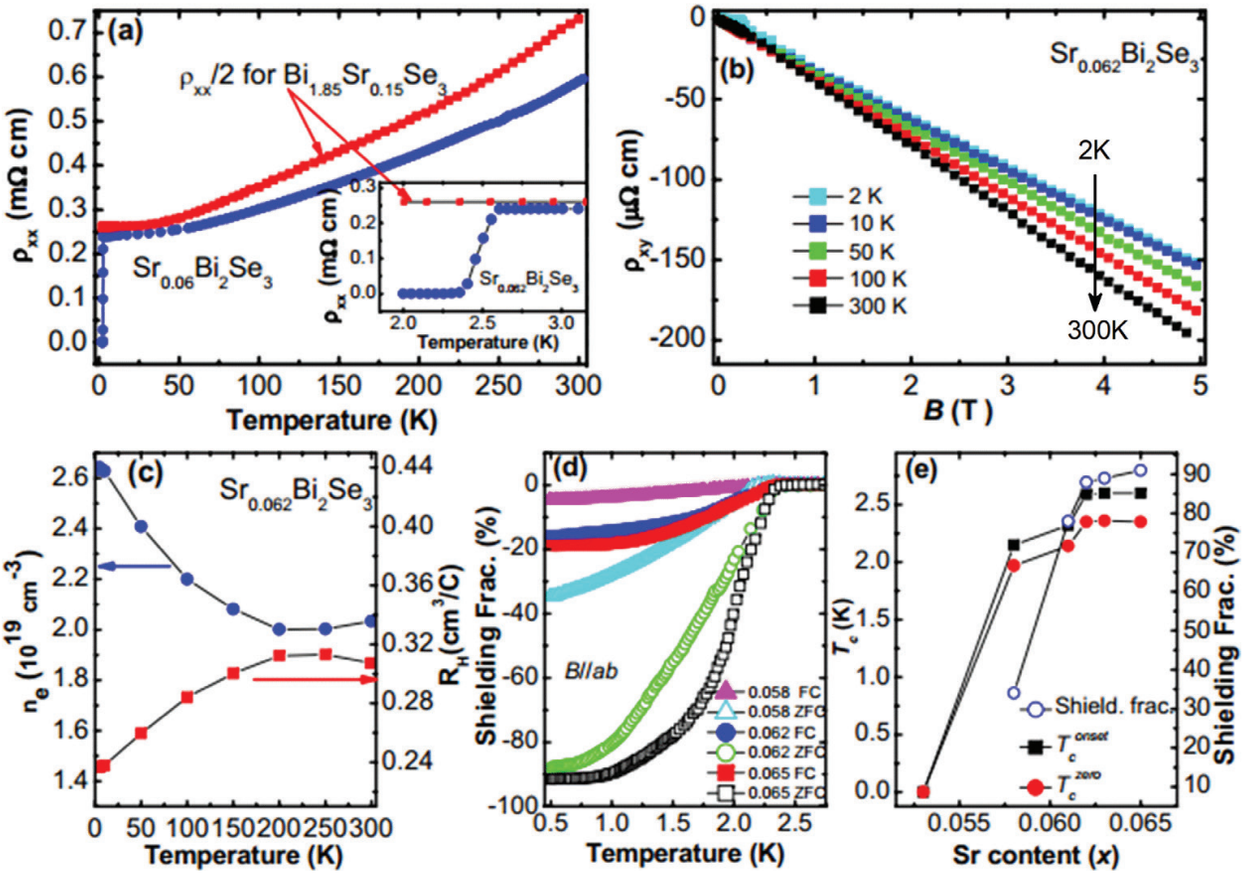

Figure 11. Superconducting properties of $Sr_xBi_2Se_3$. (a) Temperature dependence of resistivity for $Sr_xBi_2Se_3$ and $Bi_{2-x}Sr_xSe_3$. (b) Hall resistivity versus magnetic field curves measured at different temperatures. (c) Temperature dependence of estimated Hall coefficient and charge carrier density. (d) Temperature dependence of susceptibility for samples with different Sr contents. (e) Plot of T_c^{onset}, T_c^{zero}, and shielding volume fraction as a function of Sr content [7].

indices. In fact, the measured resistivity and Hall resistivity actually contain contributions from both the surface and bulk conductance when a large parallel bulk conduction channel is present. Therefore, the least confusing method is to convert resistivity into conductance to determine the Landau index because its components are additive [34]. The following equations are used to calculate conductance

$$G_{xx} = \frac{R_{xx}}{R_{xx}^2 + R_{xy}^2}, \quad G_{xy} = \frac{R_{xy}}{R_{xx}^2 + R_{xy}^2}. \tag{3}$$

After removing the nonoscillatory background, the oscillatory components are obtained and plotted as a function of 1/B. The frequencies are 146 T for longitudinal conductance and 144.8 T for Hall conductance, which are comparable to those of Bi_2Se_3 but smaller than $Cu_xBi_2Se_3$. The integer Landau index n corresponds to the valleys in ΔG_{xx}, while the valleys in ΔG_{xy} are assigned to n + 1/4 [see **Figure 13(a)** and **(c)**]. The 1/4 shift arises to match the valleys in $d\Delta G_{xy}/dB$ with the valleys in ΔG_{xx} [34]. The obtained intercepts of the linear fittings for n versus 1/B are both close to the value for an ideal Dirac system, i.e., −0.5 rather than 0 or 1 (see **Figure 13(b)** and **(d)**). Thus, it provides transport evidence for the existence of Dirac fermions in $Sr_xBi_2Se_3$ superconductor.

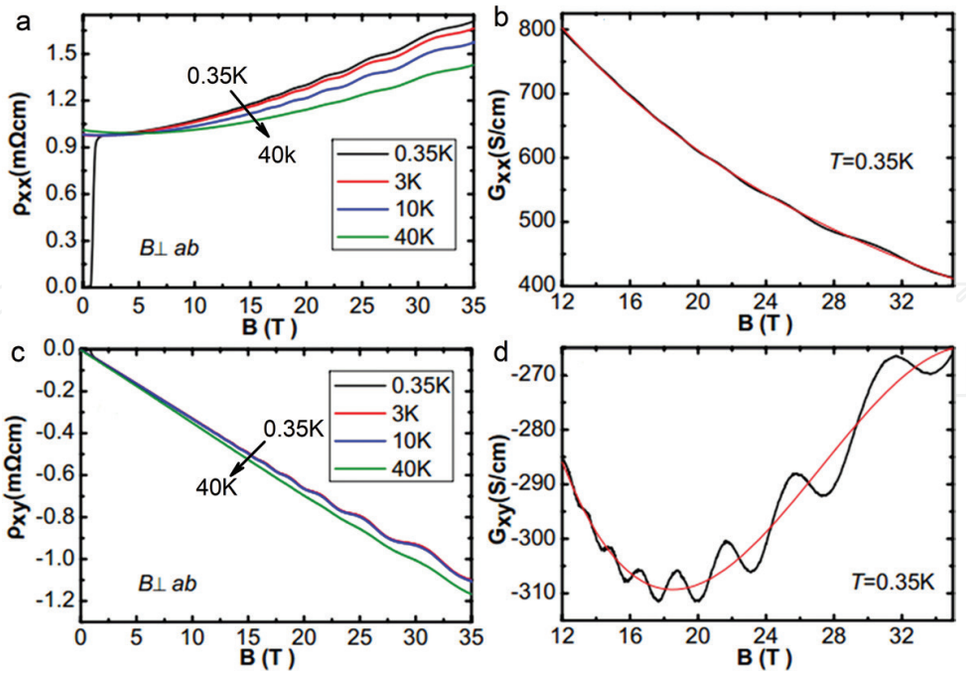

Figure 12. SdH oscillations under high magnetic field for $Sr_xBi_2Se_3$ single crystal. (a) and (c) Magnetic field dependence of resistivity and Hall resistivity at different temperatures. (b) and (d) Magnetic field dependence of the fitted longitudinal and Hall conductivity at 0.35 K [7].

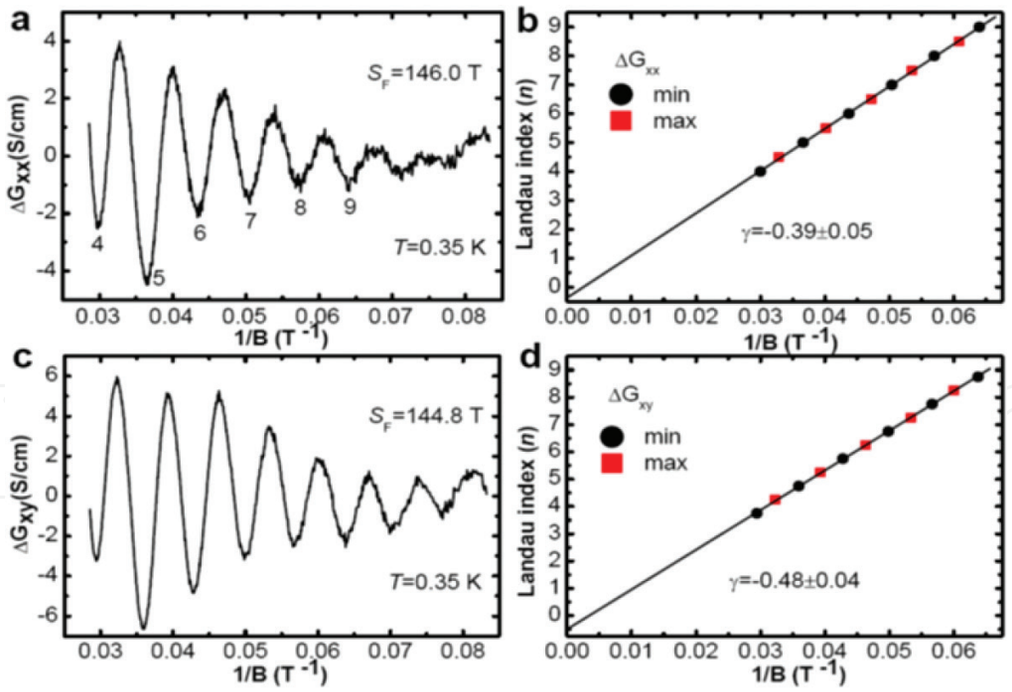

Figure 13. (a) and (c) Oscillatory component of the longitudinal and Hall conductivity at 0.35 K plotted against 1/B. (b) The Landau index n versus 1/B, where n and n + 1/2 correspond to the valleys and peaks of ΔG_{xx}. (d) n versus 1/B derived from (c), where n + 1/4 corresponds to the valleys of ΔG_{xy} [7].

The superconductivity of $Sr_xBi_2Se_3$ is very sensitive to external pressure below 1 GPa, as seen in **Figure 14(a)** and **(b)**. With the increasing applied pressure, the T_c and shielding volume fraction decrease but the normal state resistivity increases. This depression of superconductivity can be

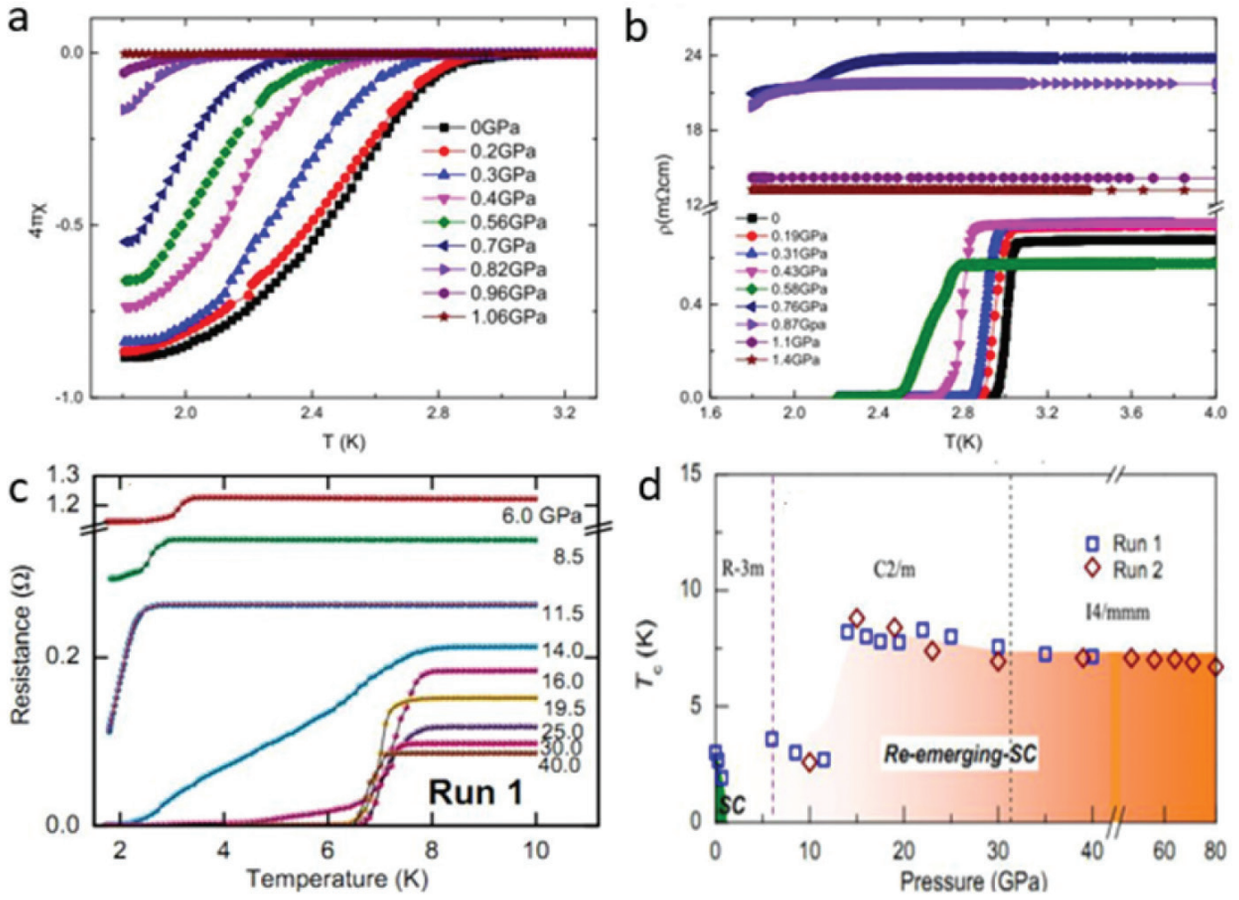

Figure 14. (a) Temperature dependence of magnetic susceptibility under different pressures. (b) and (c) Temperature dependence of resistance under high pressure. (d) The structural phase diagram on pressure for $Sr_xBi_2Se_3$ [35].

attributed to the reduction of charge carrier density, which is apparent from the normal state resistivity. However, if the pressure continues to increase, the normal state resistivity begins to decrease and a sign of superconducting transition occurs at 6 GPa. Then, the T_c^{onset} and the charge carrier density estimated from the normal state resistivity gradually increase with the increasing pressure, and T_c^{onset} reaches around 8 K when $P > 14$ GPa. But unfortunately, the T_c^{onset} remains almost constant for the pressure up to 40 GPa, although the normal state resistivity keeps decreasing. The reemerging superconductivity is very robust and the T_c^{onset} still changes little under 80 GPa [35]. In fact, the whole process contains three structural phases, i.e., R-3 m, C2/m, and I4/mmm, as seen in **Figure 14(d)**. The structural transitions and pressure-invariant T_c are very similar to the parent compound Bi_2Se_3, which needs further investigations.

3. Conclusions

The discovery of superconductivity in layered compound $Bi_4O_4S_3$ brings in a new BiS_2-based superconducting family, including the Bi—O—S compounds, Re(O,F)BiS_2, and M$FBiS_2$ superconductors. The superconducting layer is extended to $BiSe_2$ layer in $LaO_{1-x}F_xBiSe_2$ and $Sr_{1-x}La_xFBiSe_2$. The crystal structure and various superconducting properties are reviewed for selective systems. Hall effect and specific heat suggest that they are probably multiband

superconductors and can be described by BCS weak-coupling theory. Moreover, bismuth chalcogenide topological insulators can be turned into superconductors by doping, which are potential candidates for 3D topological superconductors. For example, the topological surface state of $Sr_xBi_2Se_3$ is well supported by SdH oscillations under high magnetic field. The intermediate external pressure can efficiently suppress the superconductivity, which reemerges when pressure is further increased, while Tc is nearly invariant in high-pressure region, indicating an unconventional pairing state.

Acknowledgements

We acknowledge the support from the National Natural Science Foundation of China (Grant nos. 51603207, U1532267, and 11574288).

J.S. would like to dedicate his best love to his dear wife, Lv Youyou, who always encourages and supports his research and life. Best wishes for their love and coming baby. W.Z. would like to express his special thanks to his dearest daughters, Lily and Amy.

Conflict of interest

The authors declare no competing financial interests.

Author details

Jifeng Shao[1,2] and Wenka Zhu[2]*

*Address all correspondence to: wkzhu@hmfl.ac.cn

1 TianQin Research Center for Gravitational Physics, School of Physics and Astronomy, Sun Yat-sen University, Zhuhai, China

2 High Magnetic Field Laboratory, Chinese Academy of Sciences, Hefei, China

References

[1] Yang J, Liang J, Jin D, Ying S, Tang W, Rao G. The influence of fluorine on the structures and properties of $Pr_{2-x}Sr_xCuO_{4-y}$ (x = 0.0, 0.4, 1.0). Journal of Physics: Condensed Matter. 1997;**9**:1249-1259. DOI: 10.1088/s0953-8984(97)75992-7

[2] Stewart GR. Superconductivity in iron compounds. Reviews of Modern Physics. 2011;**83**: 1589-1652. DOI: 10.1103./RevModPhys.83.1589

[3] Burrard-Lucas M, Free DG, Sedlmaier SJ, Wright JD, Cassidy SJ, Hara Y, Corkett AJ, Lancaster T, Baker PJ, Blundell SJ, Clarke SJ. Enhancement of the superconducting

transition temperature of FeSe by intercalation of a molecular spacer layer. Nature Materials. 2013;**12**:15-19. DOI: 10.1038/NMAT3464

[4] Hor YS, Williams AJ, Checkelsky JG, Roushan P, Seo J, Xu Q, Zandbergen HW, Yazdani A, Ong NP, Cava RJ. Superconductivity in $Cu_xBi_2Se_3$ and its implications for pairing in the undoped topological insulator. Physical Review Letters. 2010;**104**:057001. DOI: 10.1103/PhysRevLett.104.057001

[5] Sasaki S, Kriener M, Segawa K, Yada K, Tanaka Y, Sato M, Ando Y. Topological superconductivity in $Cu_xBi_2Se_3$. Physical Review Letters. 2011;**107**:217001. DOI: 10.1103/PhysRevLett.107.217001

[6] Lawson BJ, Hor YS, Li L. Quantum oscillations in the topological superconductor candidate $Cu_{0.25}Bi_2Se_3$. Physical Review Letters. 2012;**109**:226406. DOI: 10.1103/PhysRevLett.109.226406

[7] Liu Z, Yao X, Shao J, Zuo M, Li P, Tan S, Zhang C, Zhang Y. Superconductivity with topological surface state in SrxBi2Se3. Journal of the American Chemical Society. 2015; **137**:10512. DOI: 10.1021/jacs.5b06815

[8] Smylie MP, Claus H, Welp U, Kwok W-K, Qiu Y, Hor YS, Snezhko A. Evidence of nodes in the order parameter of the superconducting doped topological insulator $Nb_xBi_2Se_3$ via penetration depth measurements. Physical Review B. 2016;**94**:180510(R). DOI: 10.1103/PhysRevB.94.180510

[9] Mizuguchi Y, Fujihisa H, Gotoh Y, Suzuki K, Usui H, Kuroki K, Demura S, Takano Y, Izawa H, Miura O. BiS_2-based layered superconductor $Bi_4O_4S_3$. Physical Review B. 2012;**86**:220510. DOI: 10.1103/PhysRevB.86.220510

[10] Mizuguchi Y, Demura S, Deguchi K, Takano Y, Fujihisa H, Gotoh Y, Izawa H, Miura O. Superconductivity in novel BiS_2-based layered superconductor $LaO_{1-x}F_xBiS_2$. Journal of the Physical Society of Japan. 2012;**81**:114725. DOI: 10.1143/jpsj.81.114725

[11] Yazici D, Huang K, White BD, Chang AH, Friedman AJ, Maple MB. Superconductivity of F-substituted $LnOBiS_2$ (Ln=La, Ce, Pr, Nd, Yb) compounds. Philosophical Magazine. 2013;**93**:673-680. DOI: 10.1080/14786435.2012.724185

[12] Lin X, Ni X, Chen B, Xu X, Yang X, Dai J, Li Y, Yang X, Luo Y, Tao Q, Cao G, Xu Z. Superconductivity induced by La doping in $Sr_{1-x}La_xFBiS_2$. Physical Review B. 2013; **87**:020504(R). DOI: 10.1103/PhysRevB.87.020504

[13] Lin L, Li Y, Jin Y, Huang H, Chen B, Xu X, Dai J, Zhang L, Yang X, Zhai H, Cao G, Xu Z. Coexistence of superconductivity and ferromagnetism in $Sr_{0.5}Ce_{0.5}FBiS_2$. Physical Review B. 2015;**91**:014508. DOI: 10.1103/PhysRevB.91.014508

[14] Zhai H-F, Tang Z-t, Jiang H, Xu K, Zhang K, Pan Z, Bao J-K, Sun Y-L, Wen-He J, Nowik I, Felner I, Li Y-K, Xu X-F, Tao Q, Feng C-M, Xu Z-A, Cao G-H. Possible charge-density wave, superconductivity, and f-electron valence instability in $EuBiS_2F$. Physical Review B. 2014;**90**:064518. DOI: 10.1103/PhysRevB.90.064581

[15] Zhai H-F, Zhang P, Si-Qi W, He C-Y, Tang Z-T, Jiang H, Sun Y-L, Bao JI-K, Nowik I, Felner I, Zeng Y-W, Li Y-K, Xiao-Feng X, Tao Q, Zhu-An X, Cao G-H. Anomalous Eu

valence state and superconductivity in Undoped $Eu_3Bi_3S_4F_4$. Journal of the American Chemical Society. 2014;**136**:15386-15393. DOI: 10.1021/ja508564s

[16] Krzton-Maziopa A, Guguchia Z, Pomjakushina E, Pomjakushin V, Khasanov R, Luetkens H, Biswas PK, Amato A, Keller H, Conder K. Superconductivity in a new layered bismuth oxyselenide: $LaO_{0.5}F_{0.5}BiSe_2$. Journal of Physics: Condensed Matter. 2014;**26**:215702. DOI: 10.1088/0953-8984/26/21/215702

[17] Shao J, Liu Z, Yao X, Zhang L, Li P, Tan S, Zhang C, Zhang Y. Superconducting properties of $BiSe_2$-based $LaO_{1-x}F_xBiSe_2$ single crystals. EPL. 2014;**107**:37006. DOI: 10.1209/0295-5075/107/37006

[18] Li L, Xiang Y, Chen Y, Jiao W, Zhang C, Li Z, Dai J, Li Y. Superconductivity and abnormal pressure effect in $Sr_{0.5}La_{0.5}FBiSe_2$ superconductor. Superconductor Science and Technology. 2016;**29**:04LT03. DOI: 10.1088/0953-2048/29/4/04LT03

[19] Adam Phelan W, Wallace DC, Arpino KE, Neilson JR, Livi KJ, Seabourne CR, Scott AJ, McQueen TM. Stacking variants and superconductivity in the Bi—O—S system. Journal of the American Chemical Society. 2013;**135**:5372. DOI: 10.1021/ja4011767

[20] Shao J, Yao X, Liu Z, Li P, Tan S, Zhang C, Zhang Y. Bulk superconductivity in single-phase $Bi_3O_2S_3$. Physica Status Solidi RRL: Rapid Research Letters. 2014;**8**:845-848. DOI: 10.1002/pssr.201409254

[21] Shao J, Yao X, Liu Z, Li P, Tan S, Zhang C, Zhang Y. Superconductivity in $BiO_{1-x}F_{x}$-BiS_2 and possible parent phase of $Bi_4O_4S_3$ superconductor. Superconductor Science and Technology. 2015;**28**:015008. DOI: 10.1088/0953-2048/28/1/015008

[22] Okada T, Ogino H, Shimoyama J-i, Kishio K. Topotactic synthesis of a new BiS_2-based superconductor $Bi_2(O,F)S_2$. Applied Physics Express. 2015;**8**:023102. DOI: 10.7567/apex.8.023102

[23] Biswas PK, Amato A, Baines C, Khasanov R, Luetkens H, Lei H, Petrovic C, Morenzoni E. Low superfluid density and possible multigap superconductivity in the BiS_2-based layered superconductor $Bi_4O_4S_3$. Physical Review B. 2013;**88**:224515. DOI: 10.1103/PhysRevB.88.224515

[24] Yao X, Shao J, Liu Z, Zhang L, Tan S, Zhang C, Zhang Y. A comparison of the effects of Sm and Pb doping in $Bi_4O_4S_3$ superconductors. Journal of Superconductivity and Novel Magnetism. 2014;**27**:2555-2562. DOI: 10.1007/s10948-014-2624-y

[25] Liu Y, Tong P, Tan SG, Lu WJ, Li LJ, Zhao BC, Zhang SB, Sun YP. The effects of Cu doping on the physical properties of the new layered superconductor $Bi_{4-x}Cu_xO_4S_3$. Physica B. 2013;**412**:119-121. DOI: 10.1016/j.physb.2012.12.028

[26] Jha R, Awana VPS. Effect of Se doping in recently discovered layered $Bi_4O_4S_3$ superconductor. Physica C. 2014;**498**:45-49. DOI: 10.1016/j.physc.2014.01.003

[27] Nagao M, Miura A, Demura S, Deguchi K, Watauchi S, Takei T, Takano Y, Kumada N, Tanaka I. Growth and superconducting properties of F-substituted $ROBiS_2$ (R = La, Ce, Nd) single crystals. Solid State Communications. 2014;**178**:33-36. DOI: 10.1016/j.ssc.2013.10.019

[28] Yazici D, Huang K, White BD, Jeon I, Burnett VW, Friedman AJ, Lum IK, Nallaiyan M, Spagna S, Maple MB. Superconductivity induced by electron doping in $La_xM_xOBiS_2$ (M= Ti, Zr, Hf, Th). Physical Review B. 2013;**87**:174512. DOI: 10.1103/PhysRevB.87.174512

[29] Blatter G, Geshkenbein VB, Larkin AI. From isotropic to anisotropic superconductors: A scaling approach. Physical Review Letters. 1992;**68**:875. DOI: 10.1103/PhysRevLett.68.875

[30] Jha R, Kishan H, Awana VPS. Effect of hydrostatic pressures on the superconductivity of new BS_2 based $REO_{0.5}F_{0.5}BiS_2$ (RE = La, Pr and Nd) superconductors. Journal of Physics and Chemistry of Solids. 2015;**84**:17-23. DOI: 10.1016/j.jpcs.2014.12.005

[31] Liu J, Li S, Li Y, Zhu X, Wen H-H. Pressure-tuned enhancement of superconductivity and change of ground state properties in $LaO_{0.5}F_{0.5}BiSe_2$ single crystal. Physical Review B. 2014;**90**:094507. DOI: 10.1103/PhysRevB.90.094507

[32] Sasaki S, Segawa K, Ando Y. Superconductor derived from a topological insulator heterostructure. Physical Review B. 2014;**90**:220504(R). DOI: 10.1103/PhysRevB.90.220504

[33] Wang Z, Taskin AA, Frolich T, Braden M, Ando Y. Superconductivity in $Tl_{0.6}Bi_2Te_3$ derived from a topological insulator. Chemistry of Materials. 2016;**28**:779-784. DOI: 10.1021/acs.Chemmater. 5b03727

[34] Xiong J, Luo Y, Khoo YH, Jia S, Cava RJ, Ong NP. High-field Shubnikov-de Haas oscillations in the topological insulator Bi_2T_2Se. Physical Review B. 2012;**86**:045314. DOI: 10.1103/PhysRevB.86.045314

[35] Zhou Y, Chen X, Zhang R, Shao J, Wang X, An C, Zhou Y, Park C, Tong W, Pi L, Yang Z, Zhang C, Zhang Y. Pressure-induced reemergence of superconductivity in topological insulator Sr0.065Bi2Se3. Physical Review B. 2016;**93**:144514. DOI: 10.1103/PhysRevB.93.144514

IntechOpen